16th World Conference on Earthquake Engineering, 16WCEE 2017

Santiago Chile, January 9th to 13th 2017

Paper N° 1796 (Abstract ID)

Registration Code: S- K1466052004

STRESS – STRAIN RELATIONSHIP OF CONCRETE RETROFITTED WITH CARBON FIBER SHEET UNDER CYCLIC LOADING

R. Reyna(1), T. Saito(2), T. Matsui(3) and K. Hayashi(4)

(1) Doctor of Engineering., Dept. of Architecture and Civil Engineering, Toyohashi University of Technology, rreynas@uni.edu.pe
(2) Professor, Dept. of Architecture and Civil Engineering, Toyohashi University of Technology, tsaito@ace.tut.ac.jp
(3) Associate Professor, Dept. of Architecture and Civil Engineering, Toyohashi University of Technology, matsui@ace.tut.ac.jp
(4) Assistant Professor, Dept. of Architecture and Civil Engineering, Toyohashi University of Technology, hayashi@ace.tut.ac.jp

Abstract

Earthquakes are caused by a sudden release of energy from the movement between tectonic plates; besides geological faults and volcanism. As Peru is located in a high seismic hazard zone, it is necessary to improve the seismic response of buildings against earthquakes. In addition, in recent years, large scale construction of medium-rise building that use low ductility reinforced concrete wall (LDRC) has become commonplace in Peru. These walls do not have boundary columns but instead have a small quantity of reinforcing bars at each end and therefore expected to fail in flexural mode.

To improve seismic response against earthquakes, two verification tests were conducted by using carbon fiber sheet (CFS) as a retrofitting method in Toyohashi University of Technology, Japan. The first test was conducted over three LDRC walls (Without CFS, full wall retrofitted with CFS and edges retrofitted with CFS). The second test was conducted following the same retrofitted pattern of the first experiment but with a partial height retrofitted with CFS. From those tests, it was verified that carbon fiber sheets delay the concrete crushing of the wall base that occurs during flexural failure and that deformation performance was improved.

To verify the confinement effect of CFS, a third experiment was conducted using concrete samples with CFS by changing the size, shape and number of CFS layers. In total, 39 concrete samples (Circular shape: 8-ϕ150x300mm, Square shape: 9-150x150x300mm, 2-150x150x450mm, Rectangular shape: 4-150x300x300mm, 2-150x300x450mm, 5-100x300x200mm, 2-100x300x300mm, 5-100x400x200mm, 2-100x400x300mm,) were tested under compressive loading (monotonic and cyclic). From the experiment, it was confirmed that deformation performance was improved and the strength of the concrete was increased due to the confinement provided by the CFS, however the stress-strain relationship of concrete with CFS depends on the shape of the concrete sample. This study will focus on the third experiment corresponding to the circular and square shaped specimens.

A model of stress-strain relationship of concrete with CFS was proposed and compared with the experimental results. Parameters which affect the stress-strain relationship were discussed, such as: sample shape, confinement ratio, etc.

Keywords: Stress-Strain Relationship; Confinement Effect; Carbon Fiber Sheet; Seismic Retrofitting.

1. Introduction

Earthquakes are caused by a sudden release of energy from the movement between tectonic plates; besides geological faults and volcanism. As Peru is located in a high seismic hazard zone, it is necessary to improve the seismic response of buildings against earthquakes. In addition, in the last years, large scale construction of medium-rise building that use low ductility reinforced concrete wall (LDRC) has become commonplace in Peru. These walls do not have boundary columns but instead have a small quantity of reinforcing bars at each end [1] and therefore expected to fail in flexural mode.

Two experiments were conducted on low ductility reinforced concrete wall with and without carbon fiber sheet (CFS) as a retrofitting method. The first experiment was conducted in 2013 at the Toyohashi University of Technology (TUT) on three LDRC walls [2], the first wall was without CFS reinforcement, the second wall was wrapped completely with CFS and the third wall was wrapped with CFS at the edges only. A second experiment was conducted in 2014 at TUT on three LDRC walls, following the same retrofitted pattern of the first experiment but with partial retrofitting with CFS to a specified height [3].

From those tests, it was verified that the carbon fiber sheets delay the concrete crushing of the wall base that occurs during flexural failure and that deformation capacity was improved. Moreover, during the test with the retrofitted walls it was observed that the crushing of the concrete produces bulges at the base corners of the wall. Additionally, when the maximum strain on the CFS is reached, the carbon fiber sheet over the crushed concrete area fails suddenly.

In order to verify the confinement effect of the carbon fiber sheet used as a retrofitting method for concrete, a third experiment was conducted in 2015 at TUT using concrete samples with and without CFS, by changing the size, shape and number of CFS layers [4]. In total 39 concrete samples (Circular shape: 8-ϕ150x300mm, Square shape: 9-150x150x300mm, 2-150x150x450mm, 4-150x300x300mm, 2-150x300x450mm, 5-100x300x200mm, 2-100x300x300mm, 5-100x400x200mm, 2-100x400x300mm,) were tested under compressive loading (monotonic and cyclic).

From the third experiment, it was confirmed that deformation performance was improved and that strength of the concrete was increased due to the confinement provided by the CFS, however the stress-strain relationship of concrete with CFS depends on the shape of the concrete sample. This study will focus on the third experiment corresponding to the circular and square shaped specimens.

The stress-strain relationship of concrete adapted for this study is based on the modification of Darwin & Pecknold [5], Noguchi [6], Naganuma [7] and Lam & Teng's model [8-10]. Concrete with CFS confinement was modeled based on the modification of Nakatsuka's model [11,12].

2. Experimental Work

2.1 Specimens

This study is focused on circular (C) and square (S) shaped concrete samples with and without CFS under monotonic and cyclic loading [4]. The dimensions of the concrete samples and the amount of CFS ratio used to confine the concrete are shown in Table 1. Where $p_f = 2t/D$, is the amount of CFS ratio, t is the total thickness of the CFS and D is the diameter for circular shaped specimen or one side length for a square shaped specimen.

The specimen code XY-WZ: XY is the shape code of the specimen, W is the amount of CFS used to confine the specimen (0: concrete only, 2: 1 layer of CFS-1, 3: 1 layer of CFS-2, 4: 2 layer of CFS-1, 6: 2 layer of CFS-2) and Z corresponds to the special condition (C: Cyclic test, E: CFS-3 is used instead of CFS-2). Three kind of CFS were used to retrofit the specimens with CFS to confine the concrete sample and the material properties of the CFS are shown in Table 2.

Table 1 – Dimension of concrete samples and amount of CFS confinement

Specimen	b (mm)	d (mm)	h (mm)	p_f (%)
C2-0	ϕ150		300	-
C2-0C				-
C2-2				0.148
C2-3				0.223
C2-3C				0.223
C2-3E				0.217
C2-4				0.296
C2-6				0.445
S12-0	150	150	300	-
S12-0C				-
S12-2				0.148
S12-3				0.223
S12-3C				0.223
S12-3E				0.217
S12-4				0.296
S12-6				0.445
S13-0	150	150	450	-
S13-3				0.223

Table 2 – Material properties of the CFS with glue

CFS	ρ_f (g/m^2)	t (mm)	E_f (MPa)	σ_{fu} (MPa)	ε_{fu} (%)
1	200	0.111	249000	4283	1.72
2	200	0.167	249000	4681	1.88
3	300	0.163	444000	3241	0.73

2.2 Loading Program

Two types of test where conducted:

- Monotonic test, where the specimen is under compressive loading until failure.
- Static reversal loading (Cyclic Test), where the specimen is under cyclic loading until failure. Once the target strain is reached, the unloading stage starts there is until zero stress, and then the reloading continues to the next target strain.

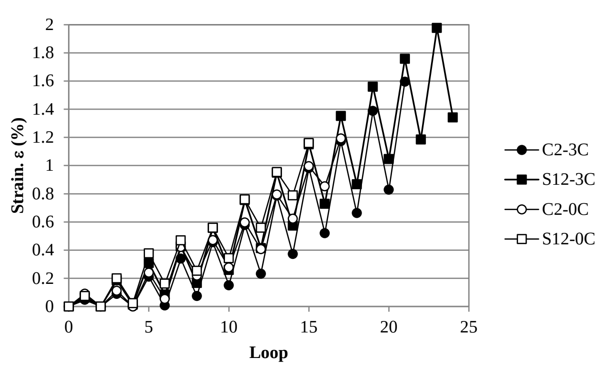

Fig. 1 – Loading pattern for cyclic test

2.3 Measuring Method

The vertical displacement of the concrete along the compressive direction was measured using displacement transducers for all the specimens, as is shown in Fig. 2. In the case of the retrofitted specimens with CFS, the horizontal strain of the CFS was measured using strain gauges. Specimens with CFS and strain gages are shown in Fig. 3.

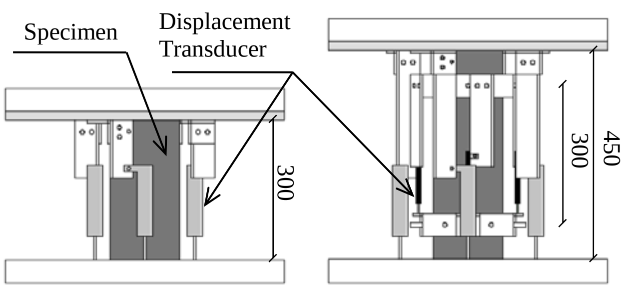

Fig. 2 – Arrangement of measuring devices (unit: mm)

Fig. 3 – Specimens with strange gages

2.4 Test Result – Circular Shaped Specimens

The circular shaped specimen C2 is 150mm in diameter and 300mm in height. Fig. 4 shows the increment in strength and the increment of deformation capacity due to CFS confinement on the concrete samples.

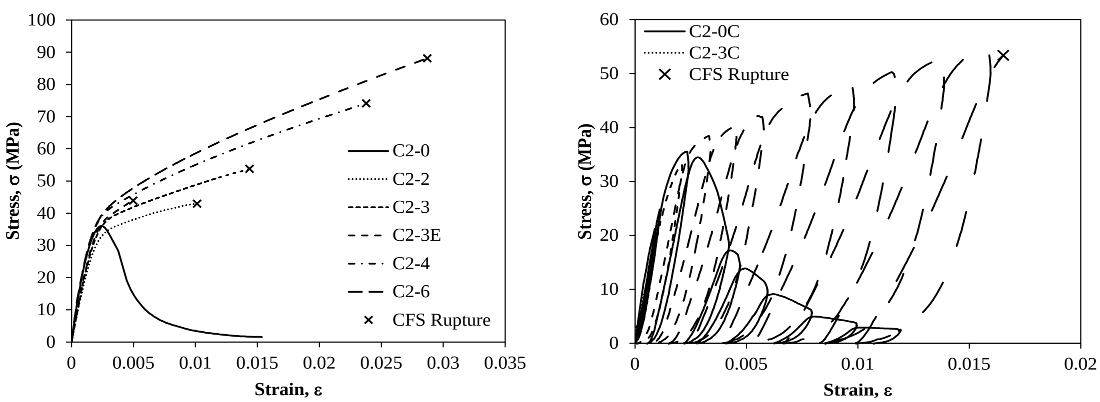

Fig. 4 – Circular shaped specimens. Left: Monotonic test, Right: Cyclic test

During the failure mode with circular shaped specimens retrofitted with CFS a sudden failure occurs when the maximum strength is reached. This can be explained as the deformation of the concrete applies about the same level of stress on the CFS. Fig. 5 shows the failure sequence: (a) shows the state of the specimen before reaching the maximum strength, (b) shows the state of the specimen when the maximum strength is reached; after this, the strength drops suddenly (c) shows the remaining core of concrete and (d) shows the state of the specimen after the crushing of concrete.

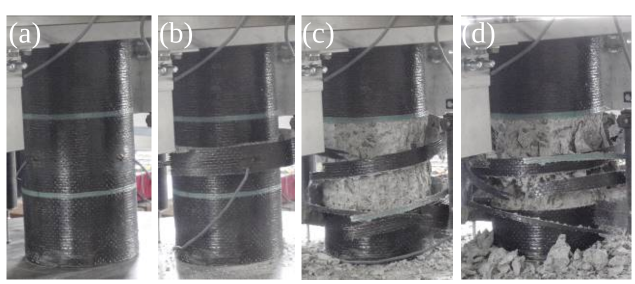

Fig. 5 – Failure mode of circular shaped specimens

2.5 Test Result – Square Shaped Specimens

The square shaped specimen has a cross section of 150mm x 150mm and heights of 300mm and 450mm for S12 and S13 respectively. Fig. 6 shows the increment in strength due to the CFS confinement on the concrete samples and the increment of deformation capacity. Moreover it can be observed that after reaching the maximum strength the specimen shows a reduction in strength.

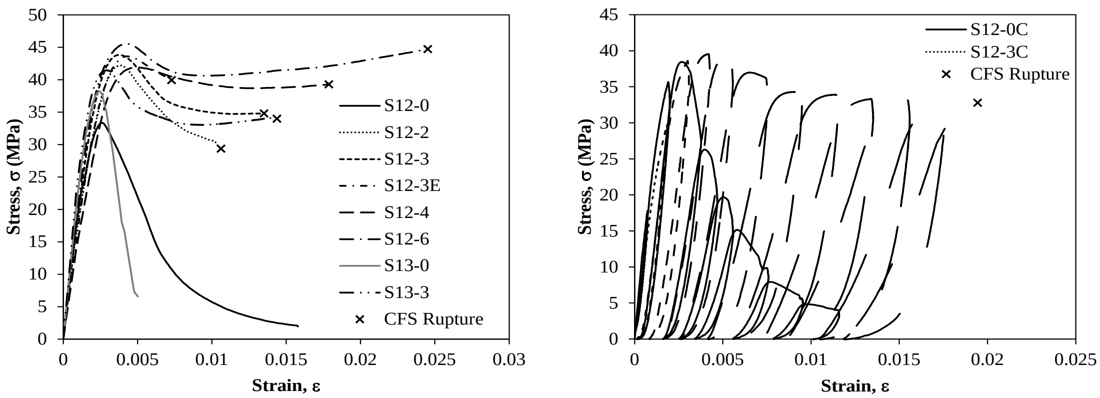

Fig. 6 – Square shaped specimens. Left: Monotonic test, Right: Cyclic test

In the failure mode with the square shaped specimen retrofitted with CFS, a two-step failure occurs; due to the stress on the CFS concentrated at the rounded corners of the specimen. Fig. 7 shows the failure sequence: (a) shows the state of the specimen before reaching the maximum strength, (b) shows the state of the specimen after the maximum strength is reached, the strength decreases and the strain deformation capacity is improved, (c) shows the state of the specimen when CFS fails first at one corner partially releasing the confinement provided by CFS and (d) shows the state of the specimen when the CFS fails at the opposite corner. This study will consider the stress-strain relationship up until the first CFS failure.

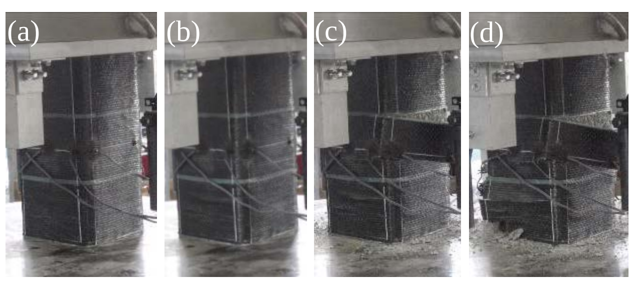

Fig. 7 – Failure mode of square shaped specimens

3. Material Model

3.1 Concrete Model

The equivalent uniaxial stress-strain curve of concrete in compression and tension shown in Fig. 8 is based on the Modified Darwin & Pecknold [5], Noguchi [6], Naganuma [7] and Lam & Teng's Model [8-10]. The envelope curve is composed by:

- $O \rightarrow M$: Suggested by Saenz et al. goes from the origin until the maximum strength of concrete f'_c (M).
- $M \rightarrow T$: Linear portion after reaching the maximum strength of concrete. The strength decreases until T-point.
- $T \rightarrow R$: Linear portion, the strength continues decreasing until R-point ($4\varepsilon_{cu}$,$0.10\, f'_c$).
- $R \rightarrow$: Flat portion where the strength remains constant at $0.10\, f'_c$ of strength.
- $O \rightarrow N$: Linear portion with E_0 slope until the maximum tensile strength of concrete.
- $N \rightarrow$: Decreasing the strength of concrete with the opening crack of concrete.

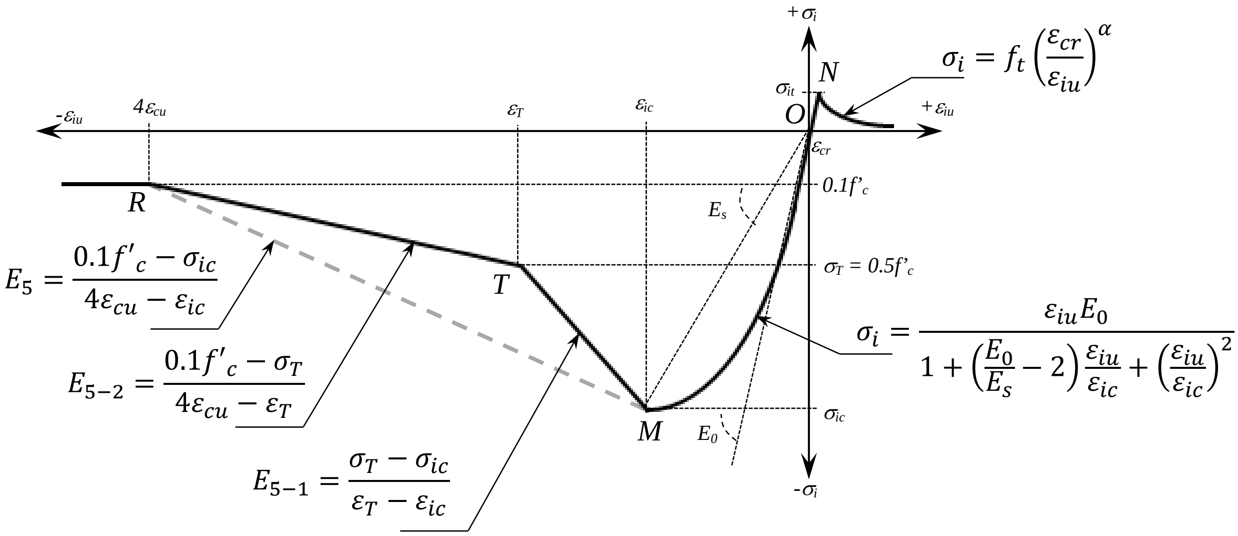

Fig. 8 – Envelope curve for concrete

Where:

- E_0: Tangent modulus of elasticity at zero stress
- E_s: Secant modulus at the point of maximum compressive stress, σ_{ic} ($E_s = \sigma_{ic}/\varepsilon_{ic}$)
- ε_{ic}: Corresponding equivalent uniaxial strain at, σ_{ic}
- ε_{cu}: Real strain at f'_c from the compression test
- ε_{cr}: Equivalent uniaxial strain at σ_{it}, where the cracking starts

The loading, unloading and reloading in compression are described From Level 1 to Level 5 as is shown in Fig. 9. For the case in which the reloading takes place during Level 3 and before reaching zero stress (P), the reloading curve goes into Level 4, oriented to the common point (C) between the unloading curve and the re-loading curve. Moreover, in case of unloading occurring over Level 4 and before reaching the common point (C), the unloading curve goes over a new Level 3, oriented to the same plastic strain (P). (See Fig. 10).

From Fig. 10, for the case in which a second unloading takes place after the concrete has been reloaded, and the unloading occurs after passing the common point (C) but has not yet reached the envelope curve, a new unloading curve is defined based on the projected point of unloading over the envelope curve.

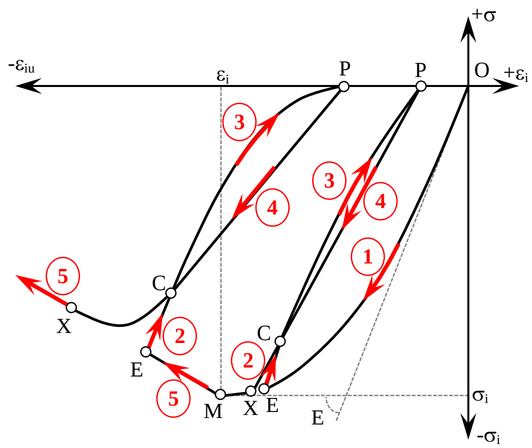

Fig. 9 – Loading, Unloading and Reloading in compression

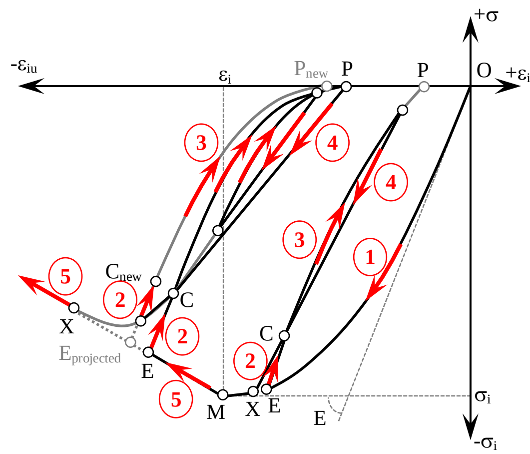

Fig. 10 – Internal cycles

Level 1: *Loading Compressive Stage: O→M*

$$\sigma_i = \frac{\varepsilon_{iu} E_0}{1 + \left(\frac{E_0}{E_s} - 2\right)\frac{\varepsilon_{iu}}{\varepsilon_{ic}} + \left(\frac{\varepsilon_{iu}}{\varepsilon_{ic}}\right)^2} \quad (1)$$

Level 2: *Unloading Compressive Stage: M→C→M (Linear)*

$$E_2 = \frac{2\sigma_{en}}{\varepsilon_{en} - \varepsilon_p} \le E_0 \quad (2)$$

Plastic Strain, (ε_P,0):

$$\varepsilon_P = \begin{cases} \left(0.145\left(\frac{\varepsilon_{en}}{\varepsilon_{cu}}\right)^2 + 0.13\left(\frac{\varepsilon_{en}}{\varepsilon_{cu}}\right)\right)\varepsilon_{cu}, & \varepsilon_{en} < \varepsilon_{ic} \\ (1.437 + 0.01 * \sigma_{ic})\varepsilon_{en} + 0.0023, & \varepsilon_{en} \ge \varepsilon_{ic} \end{cases} \quad (3)$$

Common Point, (ε_C,σ_C):

$$(\varepsilon_C, \sigma_C) = \left(\varepsilon_{en} - \frac{1}{6}\frac{\sigma_{en}}{E_2}, \frac{5}{6}\sigma_{en}\right) \quad (4)$$

Level 3: *Unloading Compressive Stage: C→P*

$$\sigma_i = a\varepsilon_i{}^n + b\varepsilon_i + c$$

$$E_P = \frac{\sigma_F}{\varepsilon_F - \varepsilon_P} \quad (5)$$

Level 4: *Reloading Compressive Stage:*

P→C (Linear), C→X (Parabolic)

$$E_4 = \frac{\sigma_C}{\varepsilon_C - \varepsilon_P} \quad (6)$$

Level 5-1: *Loading Compressive Stage: M→T*

(Linear)

$$E_{5-1} = \frac{\sigma_T - \sigma_{ic}}{\varepsilon_T - \varepsilon_{ic}} \quad (7)$$

Level 5-2: *Loading Compressive Stage: T→R*

(Linear)

$$E_{5-2} = \frac{0.1f'_c - \sigma_T}{4\varepsilon_{cu} - \varepsilon_T} \quad (8)$$

The loading, unloading and reloading in tension are described from Level 6 to Level 8.

Level 6: *Loading Tensile Stage: O→N (Linear)*

$$E_6 = E_0 \quad (9)$$

Level 7: *Crack Formation and Crack Opening: N→F*

$$\sigma_i = f_t\left(\frac{\varepsilon_{cr}}{\varepsilon_{iu}}\right)^\alpha \;,\; (\alpha = 1.0) \quad (10)$$

Level 8: *Drops linearly until Residual Deformation: F→H→F (Linear)*

$$E_8 = E_0^{\frac{\varepsilon_{cr} + r_y \varepsilon_F}{(r_y+1)\varepsilon_F}} \;,\; (r_y = 4.0)$$

$$\sigma_I = 0.9\sigma_F \quad (11)$$

$$\varepsilon_I = (\sigma_I - \sigma_F + E_8\varepsilon_F)/E_8$$

The transition from compression to tension and from tension to compression is described by Level 9 and Level 10 as is shown in Fig. 11. For the case in which an inner loop occurs in transition from Level 9 to 10 or Level 10 to 9, a linear function was proposed following a slope E_{11}; this slope can be obtained by interpolation between slope at *J*-point and E_8. (See Fig. 12).

Level 9: *Transition from Tensile Stage to Compressive Stage: H→J*

$$\sigma_i = (Ln(\varepsilon_i + a) + b)c$$

$$\sigma_J = \beta\sigma_{it} \;,\; \beta = 1.0 + 0.02\left(\frac{\varepsilon_F - \varepsilon_{cr}}{\varepsilon_{cr}}\right) \quad (12)$$

Level 10: *Transitions from Compressive Stage to the Tensile Stage: P→F*

$$E_{10} = \frac{\sigma_F}{\varepsilon_{cr} - \varepsilon_P} \quad (13)$$

Level 11: *Inner Loop in transitions from Level 9 to 10 and from 10 to 9*

(Linear)

$$E_{11} = \frac{(\varepsilon_{RT} - \varepsilon_J)(E_8 - E_J)}{\varepsilon_H - \varepsilon_J} + E_J \quad (14)$$

Where ε_{RT} is the returning point in transition from either level 9 to 10 or level 10 to 9

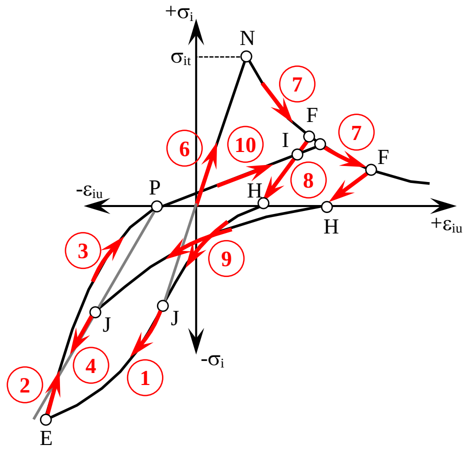

Fig. 11 – Transition from compression to tension and from tension to compression

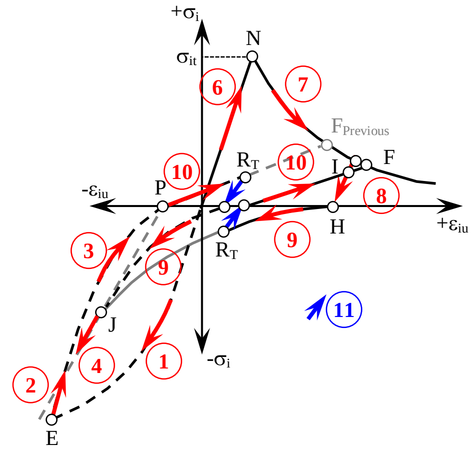

Fig. 12 – Inner loop in transition

3.2 Concrete Model with CFS Confinement

Fig. 13 shows the envelope curve for concrete with CFS confinement effect according to the Modified Nakatsuka's model [11,12] for circular and square shape sections, this model consists of an n-degree function, a linear function with slope E_{BT} and a linear function with slope E_{TR} following Eq.(15),(16) and (17) respectively.

- For $0 \le \varepsilon_c \le \varepsilon_B$:

$$\sigma_c = E_c \varepsilon_B \left(\frac{\varepsilon_c}{\varepsilon_B} - \frac{a}{n} \left(\frac{\varepsilon_c}{\varepsilon_B} \right)^n \right) \quad (15)$$

Where:

$$a = \begin{cases} 1 & (E_{BT} \le 0) \\ 1 - \frac{E_{BT}}{E_c} & (E_{BT} > 0) \end{cases} \quad n = \frac{E_c \varepsilon_B}{E_c \varepsilon_B - \sigma_B} a$$

- For $\varepsilon_B < \varepsilon_c \le \varepsilon_T$:

$$\sigma_c = \sigma_B + E_{BT} \varepsilon_B \left(\frac{\varepsilon_c}{\varepsilon_B} - 1 \right) \quad (16)$$

- For $\varepsilon_T < \varepsilon_c \le \varepsilon_R$:

$$\sigma_c = \sigma_B + E_{BT} \varepsilon_B \left(\frac{\varepsilon_T}{\varepsilon_B} - 1 \right) + E_{TR} \varepsilon_T \left(\frac{\varepsilon_c}{\varepsilon_T} - 1 \right) \quad (17)$$

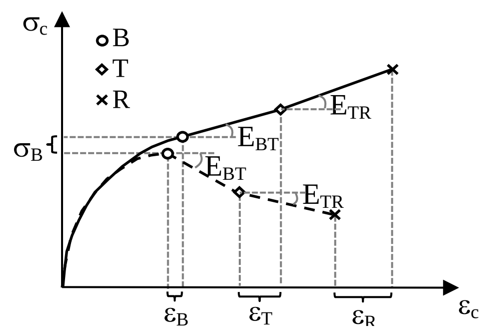

Fig. 13 – Envelope curve for concrete with CFS

Stress at B: $$\frac{\sigma_B}{F_0} = 1 + 4 C_{\sigma_B} \frac{p_f E_f \varepsilon_{fB}}{F_0} \quad (18)$$

Strain at B: $$\frac{\varepsilon_B}{\varepsilon_0} = 1 + 10 C_{\varepsilon_B} \frac{p_f E_f \varepsilon_{fB}}{F_0} \quad (20)$$

$$\varepsilon_{fB} = \begin{cases} 0.01 \left(1 - \dfrac{1}{\dfrac{F_0}{140} + 1} \right) & (F_0 \le 60) \\ 0.003 & (60 < F_0 \le 80) \end{cases} \quad (19)$$

Strain at T: $$\frac{\varepsilon_T}{\varepsilon_0} = (-0.016 F_0 + 2.7) + (-10^{-5} F_0 + 0.0016) C_{\varepsilon_T} p_f E_f \quad (21)$$

Strain at R: $$\frac{\varepsilon_R}{\varepsilon_0} = (20 \varepsilon_{fr} + 1.2) + (1000 \varepsilon_{fr} - 3) C_{\varepsilon_R} \frac{p_f E_f}{{F_0}^2} \quad (22)$$

First and second slope: $$\frac{E_{BT}}{E_{0BT}} = -0.4 + \frac{1.4}{C_{\varepsilon_{BT}} \dfrac{p_f E_f}{0.06 {F_0}^2} + 1} \quad (16) \qquad \frac{E_{TR}}{E_{0BT}} = -0.25 + \frac{0.55}{C_{\varepsilon_{TR}} \dfrac{p_f E_f}{0.06 {F_0}^2} + 1} \quad (23)$$

Where : $E_{0BT} = 1000(6 - 0.43 F_0) \quad [MPa]$

F_0 is the compressive strength of the unconfined concrete

ε_0 is the strain at F_0 for unconfined concrete

p_f is the ratio of CFS

E_f is the young modulus of CFS and E_{fr} is the rupture strain of CFS

Previous studies on the confinement effect of CFS [12] shows how shape coefficients are affected by the ratio between the effective confinement area under compression A_e and the section area A_c. following Eq. (24) and (25). The effective confinement area is contained by four parabolas as is shown in Fig. 14; with the initial slopes of the parabolas begin the same as the adjacent diagonal lines [9]. Table 3 shows the modified shape factors according to Nakatuka's procedure for R=15mm, which are different from the coefficients corresponding to R=30mm. Besides, with both coefficients and using a linear regression procedure, Nakatsuka's coefficient can be modified and interpolated for different chamfer radius as is shown in Table 3.

$$\frac{A_e}{A_c} = \frac{1 - \dfrac{\left[\frac{d}{b}(b-2R)^2 + \frac{b}{d}(d-2R)^2\right]}{3A_g} - \rho_g}{1-\rho_g} \qquad (24)$$

$$A_g = bd + (\pi - 4)R^2 \qquad (25)$$

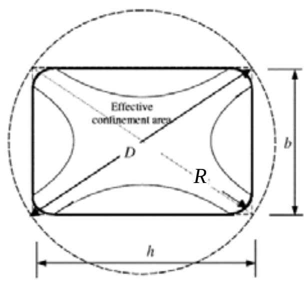

Fig. 14 – Effective confinement area

Table 3 – Modified shape coefficients

Shape Coefficients R =	15mm	30mm	Linear Regression
$C_{\sigma B}$	0.55	0.6	$C_{\sigma_B} = 0.29\dfrac{A_e}{A_c} - 0.38$
$C_{\varepsilon B}$	0.6	0.6	$C_{\varepsilon_B} = 0.6$
$C_{\varepsilon T}$	0.37	0.6	$C_{\varepsilon_T} = 1.25\dfrac{A_e}{A_c} - 0.34$
$C_{\varepsilon R}$	0.52	0.4	$C_{\varepsilon_R} = 2.62\dfrac{A_e}{A_c} - 0.97$
C_{EBT}	0.22	1.0	$C_{\varepsilon_{BT}} = 1.00\dfrac{A_e}{A_c} - 0.35$
C_{ETR}	0.13	0.4	$C_{\varepsilon_{TR}} = 1.48\dfrac{A_e}{A_c} - 0.71$

Regarding the shape coefficients for circular shaped specimens, the experimental data were used to find suitable coefficients. Fig. 15 shows the result comparison between the experimental parameter of the envelope curve for circular shaped specimens versus the calculated values by using the proposed parameters.

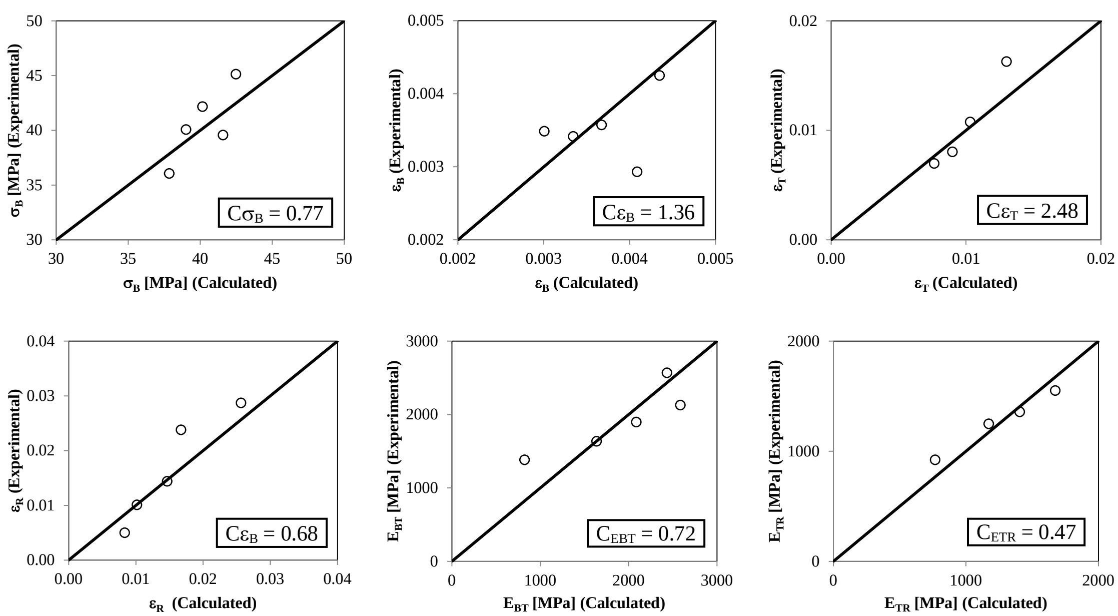

Fig. 15 – Shape coefficients for circular shaped specimens

When considering the cyclic behavior for concrete with CFS confinement, the hysteresis rules are taken as the same as for the concrete only but changing the envelope curve and the plastic strain (ε_p) must be taken following Eq. (26)

Previous studies show the experimental linear relationship between envelope unloading strain and plastic strain [10] (See Table 4); including the linear relationship found in this study, an expression for plastic strain is proposed by Eq. (26). The comparison between experimental and calculated plastic strain can be observed in Fig. 16.

Table 4 – Linear relationship between envelope unloading strain and plastic strain

Source	f'c (Mpa)	(a+cf'$_c$)	c	R^2
Reyna et al.	35.56	0.758	-0.0021	0.9982
	38.46	0.763	-0.0016	0.9997
Lam and Teng.	38.9	0.714	-0.0016	0.998
	41.1	0.703	-0.0014	0.996
Ilki and Kumbasar	32	0.713	-0.0019	0.994
Rousakis	49.5	0.737	-0.002	0.981
	65.5	0.601	-0.0015	0.981
	68.5	0.603	-0.0015	0.968
	95	0.467	-0.0013	0.999

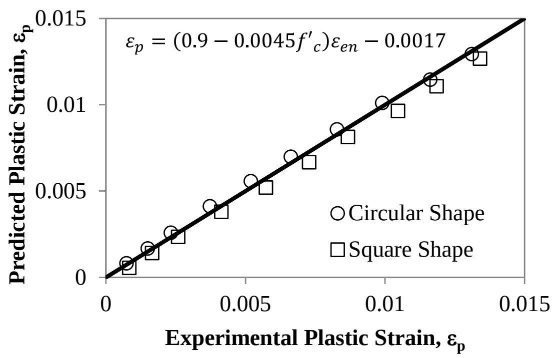

Fig. 16 – Comparison between experimental and calculated plastic strain

$$\varepsilon_P = \begin{cases} 0 \quad , \quad 0 < \varepsilon_{en} \leq 0.001 \\ [1.4(0.9 - 0.0045 * F_0) - 0.64](\varepsilon_{en} - 0.001) \quad , \quad 0.001 < \varepsilon_{en} \leq 0.035 \\ (0.9 - 0.0045 * F_0)\varepsilon_{en} - 0.0016 \quad , \quad 0.035 < \varepsilon_{en} \leq \varepsilon_R \end{cases} \qquad (26)$$

4. Experimental Results vs. Analytical Approach

4.1 Circular Shaped – Cyclic Test

Fig. 17 shows a comparison between experimental and analytical hysteresis curves for circular shaped specimens for both concrete only and concrete with CFS. The comparison shows that proposed model and the experimental result match pretty well. The strain pattern used to get the analytical curve is shown in Fig. 1. The calculated strain level for the rupture of the circular specimen of concrete with CFS is about the same level as the experimental test. Besides, the plastic strain definition for both, concrete only and concrete with CFS, has a good agreement between the experimental curve and the proposed model.

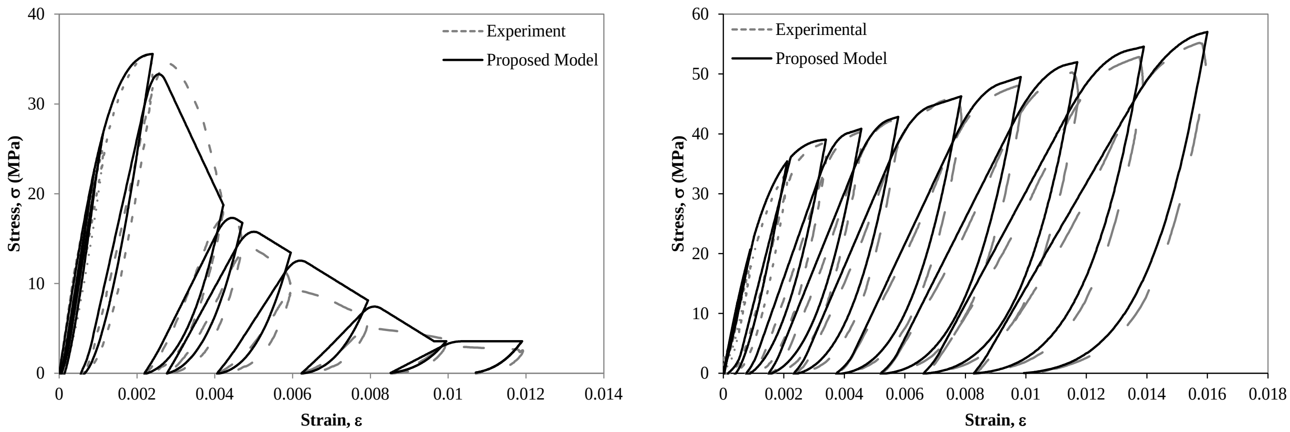

Fig. 17 – Comparison between experimental and analytical hysteresis curves for circular shape.

Left: Concrete only. Right: Concrete with CFS.

4.2 Squared Shaped – Cyclic Test

Fig. 18 shows the comparison between experimental and analytical hysteresis curves for square shaped specimens for both concrete only and concrete with CFS. The strain pattern used to get the analytical curve is shown in Fig. 1. The comparison shows that proposed model and the experimental result match pretty well. The analytical model gives a lower strain level for the rupture of the square shaped specimen of concrete with CFS, but when it is compared with the monotonic curve it has about the same strain level for the rupture of the CFS during the test.

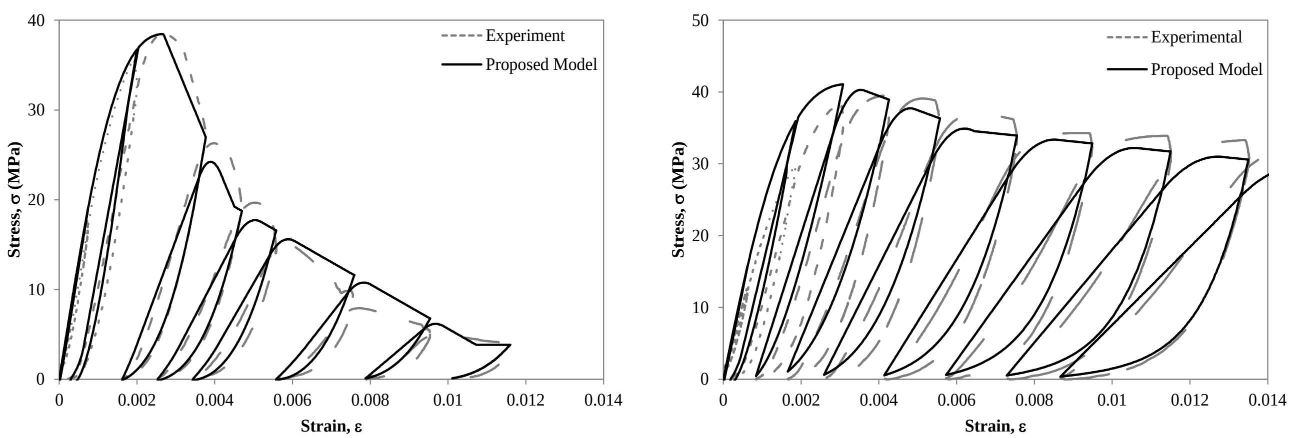

Fig. 18 – Comparison between experimental and analytical hysteresis curves for square shape.

Left: Concrete only. Right: Concrete with CFS.

5. Conclusions

- Carbon fiber sheet helps to improve the deformation capacity of the circular and rectangular concrete samples under monotonic and cyclic loading, in other words, the ductility and energy dissipation of concrete retrofitted with CFS is improved in comparison with the non-retrofitted samples.
- Circular shaped specimens retrofitted with CFS shows a significant increment of the maximum strength until the failure of the CFS.
- Square shaped specimens retrofitted with CFS shows a small increment of the maximum strength. After reaching the maximum strength, the specimen shows a reduction in strength.

- Proposed model for both, concrete only and concrete with CFS, shows a good approach in comparison with the experimental curves.
- Further studies of the shape coefficients for square and circular shaped specimens should be extended by increasing the data base to calibrate the coefficients considering a large range of concrete types and CFS.

6. Acknowledgments

This paper is part of the doctoral dissertation of the main author presented to the Graduate School of Engineering at Toyohashi University of Technology, Japan. The main author would like to thank the Japanese Government for the MEXT scholarship during his doctoral studies. Last but not least, to the students of Toyohashi University of Technology, Sakai T., Suzuki K., Tachibana K., Kanazawa Y. for their valuable support during the experimental test.

7. References

[1] Zavala C., et al., (2013): Cyclic behavior of low ductility walls considering perpendicular action. *Journal of Disaster Research*, 8(6), 312-319.

[2] Matsui T., Saito T. and Reyna R., (2014): Basic study on reinforced concrete shear walls without boundary columns retrofitted by carbon fiber sheets. *Journal of Disaster Research*, 9(6), 1008-1014.

[3] Matsui T. and Saito T., (2017): Structural performance of rectangular reinforced concrete walls retrofitted by carbon fiber sheets. *Technical Paper No. 0004*, 16th World Conference on Earthquake Engineering, Santiago, Chile.

[4] Reyna R., Saito T., Matsui T. and Hayashi, K., (2016): Confinement effect of concrete with carbon fiber sheet reinforcement under monotonic loading. *International Journal of Structural and Civil Engineering Research*, 5(4), 250-257.

[5] Darwin D., Pecknold D.A.W., (1974): Inelastic model for cyclic biaxial loading of reinforced concrete. *Technical Report SRS-409*, Civil Engineering Studies, University of Illinois, USA.

[6] Noguchi H. and Kashiwazaki T., (2004): FEM analysis of structural performance deterioration of RC elements subjected to seismic reversed cyclic shear. *Technical Paper No. 672*, 13th world Conference on Earthquake Engineering, Vancouver, B.C., Canada.

[7] Naganuma K., Yonezawa K., Kurimoto O. and Eto H. (2004): Simulation of nonlinear dynamic response of reinforced concrete scaled model using three-dimensional finite element method. *Technical Paper No. 586*, 13th World Conference on Earthquake Engineering, Vancouver, B.C., Canada.

[8] Lam L. and J.G. Teng., (2003): Design-oriented stress–strain model for FRP-confined concrete. *Construction and Building Materials*, 17(6), 471-489.

[9] Lam L. and J.G. Teng., (2003): Design-oriented stress–strain model for FRP-confined concrete in rectangular columns. *Journal of Reinforced Plastics and Composites*, 22(12), 1149-1186.

[10] Lam, L. and J.G. Teng., (2009): Stress–strain model for FRP-confined concrete under cyclic axial compression. *Engineering Structures*, 31(2), 308-321.

[11] Nakatsuka T., Kenichi K. and Kinya T., (1998): Stress–strain characteristics of confined concrete with carbon fiber sheet. *Concrete Research and Technology*, 9(2), 65-78.

[12] Reyna R., Saito T., Matsui T. and Hayashi K., (2016): Monotonic stress-strain relationship of concrete with carbon fiber sheet confinement. *Proceedings of the Japan Concrete Institute Annual Convention*, Hakata, Japan.